Direct Synthesis of Graphene on Silicon Oxide by low temperature Plasma Enhanced Chemical Vapor Deposition

R. Muñoz*[1], L. Martínez[1], E. López[1], C. Munuera[1], Y. Huttel[1] and M. García-Hernández[1]

[1] Materials Science Factory, Instituto de Ciencia de Materiales de Madrid, (ICMM-CSIC), Sor Juana Inés de la Cruz 3, E-28049, Madrid, Spain

*e-mail: rmunoz@icmm.csic.es

Keywords: graphene, plasma, synthesis, CVD, dielectric substrates

Abstract

Direct graphene growth on silicon with native oxide using Plasma enhanced Chemical Vapour Deposition at low temperatures [550 ºC -650 ºC] is demonstrated for the first time. It is shown that fine tuning of a two step synthesis with gas mixtures C_2H_2/H_2 yield monolayer and few layer graphene films with controllable domain size from 50 nm to more than 300 nm and sheet resistance ranging from 8 k ·sq^{-1} to less than 1.8 k ·sq^{-1} . Differences are understood in terms of the interaction of the plasma species -chiefly atomic H- with the deposited graphene and the native oxide layer. The proposed low temperature direct synthesis on an insulating substrate does not require any transfer processes and improves compatibility with current industrial processes.

Introduction

The recent history of graphene began in 2004[1] with its isolation from Highly Oriented Pyrolytic Graphite by mechanical exfoliation. The measurements performed on the isolated flakes confirmed the exceptional electronic properties of the material, not only in monolayer graphene but also in thicker layers.[1-3] Progressively, important studies were carried out evaluating the physical properties of the material and confirming its impressive optical,[4] thermal[5] and mechanical properties.[6] The combination of its superlative properties suggested that graphene could replace and increase the functionalities of current materials in many applications.[7, 8] However, the integration of

Corresponding Author: Tel: 0034 913349000, ext: 302
E-mail: rmunoz@icmm.csic.es (Roberto Muñoz)

graphene in existing devices relies on the development of scalable and compatible methods to produce large area graphene films without degrading their properties. The first developed method, simultaneous to mechanical exfoliation, was the epitaxial growth on (0001) SiC wafers by sublimation of the Si , a method well suited for electronic applications.[9] However, sublimation methods are limited to SiC substrates and also require very high temperatures. Presently, growth by catalytic chemical vapor deposition (CCVD) has become the most popular and scalable approach for graphene film synthesis.[10] Regarding CCVD methods, growth of graphene has been reported at temperatures around at 850ºC[11]-750ºC[12] when using acetylene as precursor. However the unavoidable transfer process is an important drawback. During the transfer, graphene is separated from the metal catalyst and laid onto a target substrate which usually leads to damage and contamination of the layers.[13, 14] In this scenario, the development of direct, catalyst free, scalable and clean production of graphene films on arbitrary substrates is an important target to integrate graphene in current technologies.

Direct pyrolytic CVD deposition has been accomplished at temperature >1000 ºC on several surfaces other than SiC such as Si_3N_4,[15, 16] Al_2O_3,[17-19] graphite,[20] h-BN,[21-23] SiC,[24] $SrTiO_3$,[25] Ge,[26, 27] fused silica or quartz glasses.[28-32] Those materials have demonstrated potential for a broad range of daily life applications. [28-33] Similarly, given that Si based electronic technology is the established standard, it would extremely interesting to grow graphene on SiO_2 so as to integrate graphene in Si-based devices. Many approaches have been recently developed in this area but the high growth temperature required in these protocols -typically over 1100 ºC[29, 34-40] poses some problems derived from the poor thermal stability of the silicon oxides on Si wafers during deposition. Among them, desorption of SiOx from the exposed surface[34] and diffusion of carbon or silicon species from the interface onto the thermally grown oxide,[29] are well known phenomena that were demonstrated to play an undesirable role on the structure and quality of the deposited graphene film. These effects are even more pronounced in Si wafers with thin oxide layers (less than 90 nm)[29] that, in turn, are an important issue in CMOS technologies.[41]

In order to manage the stability issue of the SiO_2/Si wafer and the need to avoid metal contamination, plasma assisted CVD (PE-CVD) should be considered as an alternative approach to direct deposit graphene at lower T. Several studies were reported on the grown of graphene by PE-CVD over Si/SiO_2 with thick (250-300 nm) and medium oxide layers,[42, 43] resulting in bilayer or few layer graphene with direct

application in nano-devices.[44, 45] To the best of our knowledge, systematic studies on the growth and demonstration of monolayer graphene on ultrathin or native silicon oxide layers by PE-CVD are missing. The task is not an easy one as a growth protocol on this substrate would certainly require an exquisite control of the interaction with the native oxide.

In this work, we successfully address the direct growth of graphene on silicon wafers with ultrathin native oxide layer by remote Electron Cyclotron Resonance Chemical Vapour Deposition, r-(ECR-CVD) for the first time. This plasma source provides higher efficiency in the dissociation of gas species than others, and are well suited for deposition on large areas.[46] We use a two-step process to separately control the nucleation and growth stages of the graphene film,[42, 47] enabling the fine tuning of grain size and thickness. The morphology, structure, composition and conductive properties of the resulting layers have been fully characterized. The substrate topography was also analyzed after deposition to confirm its stability under plasma environment.

Experimental

Graphene synthesis

Plasma assisted r-(ECR-CVD) technique was used for the graphene synthesis from C_2H_2/H_2 gas mixtures. The ASTEX AX 4500 ECR system employed consists of a microwave power source, a two zone chamber and a two stage pumping system (see supplementary fig. S5).[48] The gas flow is turbulent in plasma environment,[49] being the flow direction perpendicular to the sample surface. High resistivity (=3000 ·cm, p doped) silicon wafers (111) with native oxide were used as substrates. The two-step process used for graphene formation is aimed at separately controlling graphene nucleation and growth stages. In the first step, high quality graphitic seeds were nucleated with controlled coverage and density. In the second step, the edge-growth was promoted from the nucleated seeds up to graphene film formation. As demonstrated in our previous work,[47] high H_2 flow is beneficial to enhance the crystallinity of the deposits and to keep the nucleation density low. We have used the maximum H_2 flow (50 sccm) allowed by our experimental set up and H_2 flow and partial pressure (P_{H2} = $5.2 \cdot 10^{-2}$ mbar) were kept constant throughout the study. Also, the plasma power (200 W) is constant in all experiments. In order to optimize the quality of the graphene

fabrication, a temperature range from 550 ºC to 650 ºC was studied for different C_2H_2 gas flows (and, thus, different gas pressure ratio P_{H2}/P_{C2H2}). For each temperature (T), the C_2H_2 flow was tuned for nucleation (from 0.9 to 0.34 sccm) for a given time (t_1) and subsequently varied (from 0.8 to 0.24 sccm) for the growth step that takes a longer time (t_2). Once the nucleation and growth processes were finished, post-growth annealing of continuous films at 650 ºC was carried out in high vacuum (HV, 10^{-6} mbar) for two hours in order to improve the final properties of the films.

Graphene characterization

Atomic force microscopy (AFM) measurements were performed with a commercial head and software from Nanotec[50] operated at room temperature. Two different operation modes were employed: dynamic mode, exciting the tip at its resonance frequency (~75 kHz) to acquire topographic information of the films grown and contact mode to sweep away the graphene deposits and measure the thickness. Raman spectroscopy was carried out by a confocal Raman microscope (Witec alpha-300R). Raman spectra were obtained using a 532 nm excitation laser and a 100x objective lens (NA = 0.9). The incident laser power was 1 mW. X-ray Photoelectron Spectroscopy (XPS) was carried out using a PHOIBOS 100 1D electron/ion analyzer with a one dimensional delay line detector and monochromatic Al K anode (1486.6 eV). C_{KVV} was recorded with pass energy of 15 eV and a step of 10 meV. The binding energy (BE) scale was calibrated with respect to the C 1s core level peak at 285 eV. An annealing at 580 ºC for one hour was carried out in the ultra-high vacuum (UHV) chamber of the XPS (base pressure $< 2 \cdot 10^{-10}$ mbar) to compare the structure of carbon in the films before and after the annealing. The sheet resistance of the continuous films was characterized by four point probe measurement (JANDEL RMS2 Universal Probe) with continuous current (from 1 to 100 μA).

Results and discussion

In each run, a two step synthesis takes place. Firstly, we nucleate graphene seeds at a given temperature T and P_{H2}/P_{C2H2} ratio for a few minutes (t_1). Secondly, we varied the pressure relation P_{H2}/P_{C2H2} by modifying the C_2H_2 flow for a growth step during a time (t_2) to enlarge the nuclei from their edges till conforming a continuous film. During our

two step synthesis, in both steps, there exist a competition between the nucleation from carbon precursor and etching of the carbon deposit by H_2/H the plasma species. The relation H_2/C_2H_2 has to be finely tuned to avoid a too high nucleation density due to an excess of C or the disappearance of the deposit, due to too much hydrogen. The optimization of the C_2H_2 flow results in the deposition of crystalline graphene in a short time during the nucleation step leading to a low nucleation density while, in the second growth step, we optimize the C_2H_2 flow to grow only from the edge of the previously deposited nuclei. It should be emphasized here that if there were no deposited nuclei the growth would not occur in the second step in our experimental time window.

First step: Graphene nucleation on Si/SiO_x

In order to optimize the synthesis of graphene layers, control of the seed crystal structure and seed density is a must during the first step of the synthesis. The structure of nucleated seeds should be purely graphenic in nature and monolayer. The nucleation density, i. e. the number of seeds per unit area, should be as small as possible, because this parameter determines the final domain size. However, there is an intrinsic experimental limitation to assess the quality of a low density seeding as the amount of deposited carbon is below the detection limit of most of the techniques employed. Even if the nucleation time (t_1) is increased so as to drastically increase the density of nuclei, the small size of the individual nuclei makes the characterization of their structure and thickness difficult. To overcome this difficulties, we applied a short two-step process with a growth time shorter than the typically used to deposit a continuous film in a complete synthesis (t_2). This strategy has demonstrated good results on other substrates,[47] and is suitable to accomplish the assessment of the nucleation density, structure and number of layers. Moreover, in this way it can be verified whether the growth takes place from the edges or not. Figures 1, 2 and 3 show some representative examples of the graphenic layers grown on Si/SiO_x substrates with different experimental conditions.

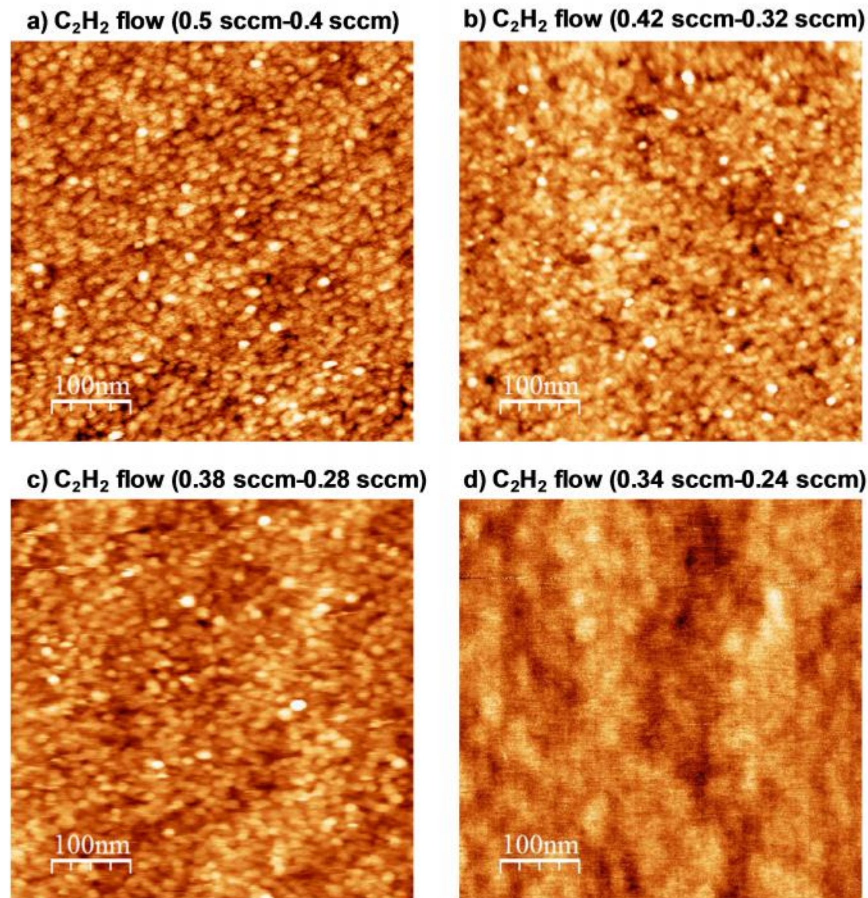

Fig. 1 AFM topographic images of graphene nuclei at 650 ºC, $P_T = 5.4\times10^{-2}$ mbar, P = 200 W, H_2=50 sccm, t_1= 5 min t_2= 90 min. Vertical scale: 0-3 nm. a) C_2H_2 flow: 0.5 sccm in nucleation and 0.4 sccm in growth step. b) C_2H_2 flow: 0.42 sccm in nucleation and 0.32 sccm in growth step. c) C_2H_2 flow: 0.38 sccm in nucleation and 0.28 sccm in the growth step. d) C_2H_2 flow: 0.34 sccm in nucleation and 0.24 sccm in the growth step. In this experiment there are no detectable nuclei.

Figure 1 presents the graphene nuclei obtained at the highest explored temperature (650 ºC). Four different C_2H_2 flows are compared (Fig. 1 (a), (b), (c), (d)) in order to assess their influence on the synthesis (nucleation). Above a threshold C_2H_2 flow of 0.38/0.28 sccm (fig. 1(c)), the seed density is very high, within the same order of magnitude (fig. 1(a) and (b)) and the substrate is completely covered with small grains. The lateral size of the deposited nuclei is around 20 nm. Below this threshold, the seed deposition does not occur (fig. 1(d)) and the substrate surface can be observed. In conclusion, there is a lack of control on the nucleation density at this temperature.

At a lower growth temperature (600 ºC), the nucleation density decreases noticeably and the grain size increases simultaneously as depicted in figure 2. Indeed, the C_2H_2 flow has been increased in order to partially compensate the reduction of the reaction rate. As observed in Fig. 2(b) and Fig. 2(c), the lower the C_2H_2 flow the lower seed density (within the same order of magnitude) and the larger island sizes are observed. The height profiles extracted from the AFM images confirm that the overall nuclei thickness is less than 1.5 nm. At this temperature the interaction with the substrate and the adsorption of the carbon precursors is less efficient than at 650 ºC (see fig.1). The best deposition conditions at 600 ºC were found for the lower C_2H_2 flow (0.6sccm-0.5sccm) (Fig. 2(c)). At these conditions, the lateral size of the nuclei surpasses 50 nm - without completing the film- while maintaining the thickness. No further reduction of the nucleation density was obtained for lower C_2H_2 flow. The stability of the oxide surface is demonstrated in figures S1 and S2. Figure 3 shows the graphene nuclei obtained at the lowest temperature explored (550 ºC).

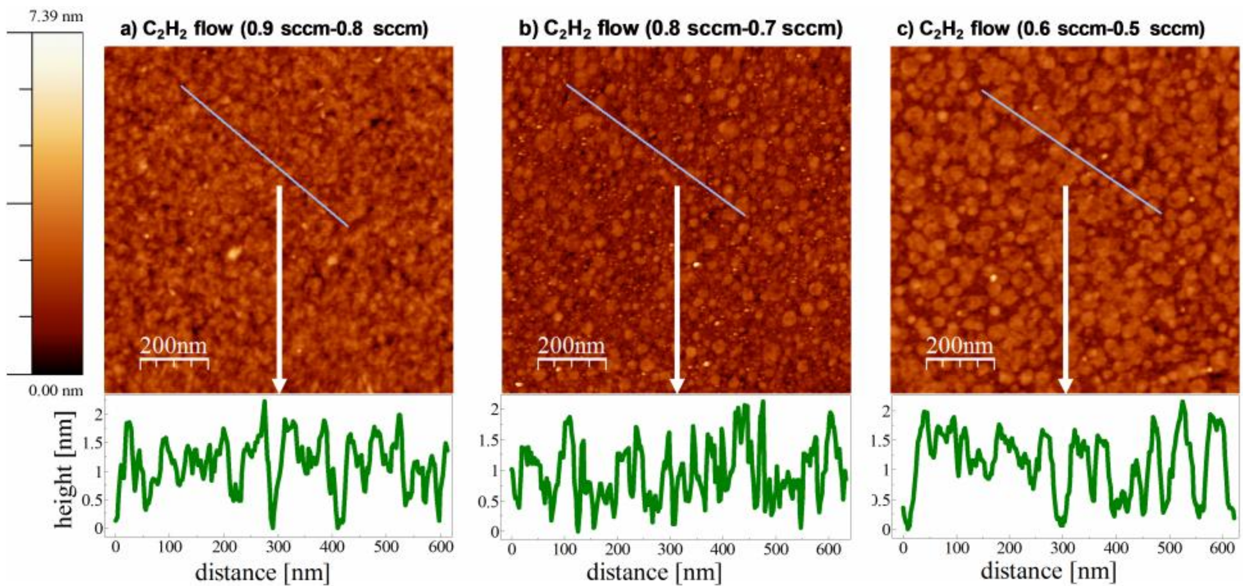

Fig. 2 AFM topographic images of the graphene nuclei and corresponding profiles at 600 ºC, $P_T = 5.4\times10^{-2}$ mbar, P = 200 W, $H_2 = 50$ sccm, $t_1 = 5$ min, $t_2 = 150$ min. a) C_2H_2 flow: 0.9 sccm in the nucleation and 0.8 sccm in the growth step. b) C_2H_2 flow: 0.8 sccm in the nucleation and 0.7 sccm in the growth step. c) C_2H_2 flow: 0.6 sccm in the nucleation and 0.5 sccm in the growth step.

Two different C_2H_2 flows are compared in order to assess the influence of the C_2H_2 pressure, without degrading the graphitic structure of the nuclei. For C_2H_2 flows similar to those previously used at higher temperature in Fig. 2(a) and 2(b), the nuclei density in Fig. 3(a) and (b) at 550 ºC is more than one order of magnitude lower than at 600 ºC. Also the nucleation density and the size of the nuclei have been found to increase with the C_2H_2 flow in figure 3(a) in comparison with fig. 3(b), up to 100 nm in some crystals. The increase of C_2H_2 flow in the nucleation step from 0.8 to 0.9 promotes a moderately increase of the nucleation density for a particular nucleation time (30 nuclei/μm^2). Also, the increase of C_2H_2 flow from 0.7 to 0.8 sccm renders an increase of the grain size during a given growth time. The height profiles displayed in figure 3(a) and (b) evidenced that, despite the different graphene nuclei sizes, for both experimental conditions, the thickness of the nuclei remained below 1 nm, resembling the features of monolayer graphene on quartz.[47] During the synthesis process, the SiO_x surface was not affected in terms of surface roughness (see supplementary figure S3), which means that the oxide surface endures the graphene fabrication process. The fact that nucleation density decreases at lower temperatures is somehow counter intuitive as a lower temperature inhibits surface kinetic processes and decreases the mobility of carbon adatoms, which should promote higher density of nuclei. However, this is not the only process that takes place when growing and other mechanisms can be present. Indeed, the nature of the substrate plays an important role. In our case, the deposit is being carried out on a SiO_2 surface that interacts with the gases and the deposit in several ways. In particular, the cracking of the carbon bond of C_2H_2 at temperatures higher than 600 °C has been reported to occur on silicon based surfaces.[51] The resulting monomers, CH_x, have higher sticking coefficient than dimmer hydrocarbons, C_2H_y and, consequently, their mobility is lower.[52, 53] Also, simultaneously, an activation of the SiO_2 surface takes place in presence of atomic hydrogen resulting in the desorption of some chemical groups, i.e. H_2O, and the appearance of dangling bonds.[47] This process is favoured at higher temperatures and it is followed by a chemical absorption that limits the mean free path of the species running on the surface. This mechanism is supressed when the graphitization starts, the chemical interaction with the substrate is no longer favoured and, consequently, the C-C bonding prevails.[54] From our results, it appears that the expected increased mobility as the temperature increases does not compensate the concomitant competing mechanisms and the nucleation density increases as the temperature is raised.

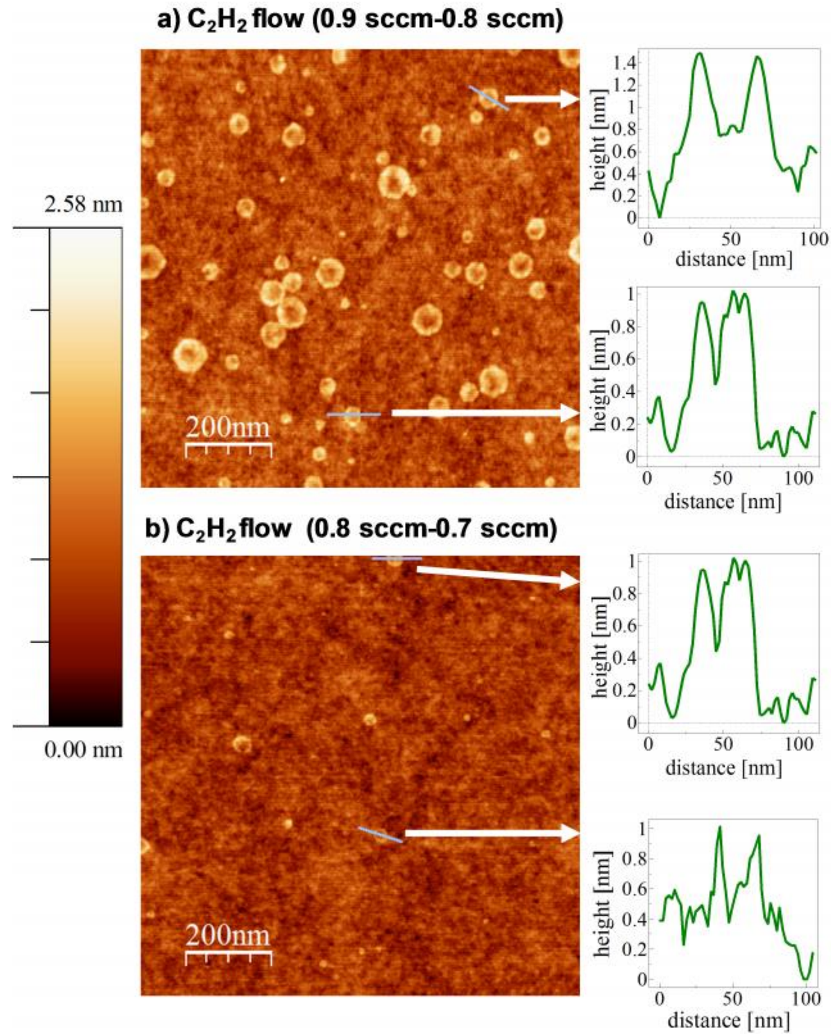

Fig. 3 AFM topographic images of the graphene nuclei and corresponding profiles at 550 ºC, $P_T = 5.4 \times 10^{-2}$ mbar, P = 200 W, H_2 = 50 sccm, t_1 = 5 min, t_2 = 150 min. a) C_2H_2 flow: 0.9 sccm in the nucleation and 0.8 sccm in the growth step. b) C_2H_2 flow: 0.8 sccm in the nucleation and 0.7 sccm in the growth step.

Second Step: Domain size enlargement and thin film deposition

After optimization of the nucleation procedure at each temperature, the enlargement of the nuclei follows up to completing the deposition of a continuous film. As first approximation, we choose the best conditions found for the nucleation, i.e. 550 ºC with

a C_2H_2 flow of 0.9 sccm in the nucleation and 0.8 sccm in the growth step (figure 3(a)), and extended the growth time (t_2). Figure 4(a) shows the submonolayer coverage of the graphene flakes. The longer t_2 (seven hours) enable the creation of graphene domains up to 300 nm in lateral size. Flake thickness, as shown in Figure 4(b), are below 1 nm, corresponding typically to a monolayer of graphene. The coalescence of the domains occurred without additional vertical growth at the grain boundaries as it is observed in quartz at 650 ºC.[47] Figure 4(c) depicts the morphology of a continuous film after completing the growth step (t_2) for 10 hours (note the homogeneity of the film in the image). Even though the vertical growth between grain boundaries was prevented, the surface of the film is not completely flat. The stitching at most grains becomes apparent, along with lack of continuity in some others (darker contrast, see also supplementary fig. S6). Figure 4(d) presents the corresponding Raman spectra of the samples displayed in figures 4(a) and 4(c), in this case before and after annealing the sample. The Raman spectrum from submonolayer coverage in blue shows the characteristic graphene peaks. The intensity ratio I_{2D}/I_G is between 1 and 2 and the 2D peak possesses a symmetric Lorentzian profile with FWHM of 38 cm^{-1}. The high value of the ratio I_D/I_G 1 is due to the high density of grain boundaries. Along with the grain boundaries, another source of defects could arise from the hydrogen enriched atmosphere during deposition, which functionalizes the graphene grains and boundaries, inducing some sp^3 hybridization in the corresponding carbon atoms.[55] The Raman spectrum in black from the continuous film in figure 4(c) shows similar results with a small decrease of the I_{2D}/I_G ratio and increase of the I_D/I_G ratio maybe related to a slight increase of defects density. The continuity of the film in figure 4(c) was confirmed by four point probe measurements. The average sheet resistance was around 15 k ·sq^{-1}. This high value can be related to these aspects mentioned, namely, incomplete stitching in some grain boundaries due to randomly oriented grains and functionalization.[56] This resistance decreased to 8 k ·sq^{-1} after annealing the sample at 650 ºC in vacuum at 10^{-6} mbar. This value are much lower than those reported in the literature for low temperature procedures.[42] It is worth mentioning that the resistance should decrease even more after annealing the samples at higher temperature or increased time. After annealing, I_D/I_G ratio of the Raman spectrum in red, figure 4(d), also decreases from approximately 1.1 to 0.9. This

could be related to H desorption from the film inducing a conversion from sp^3 to sp^2 hybridization in the carbon atoms as observed in graphene deposits on quartz.[47]

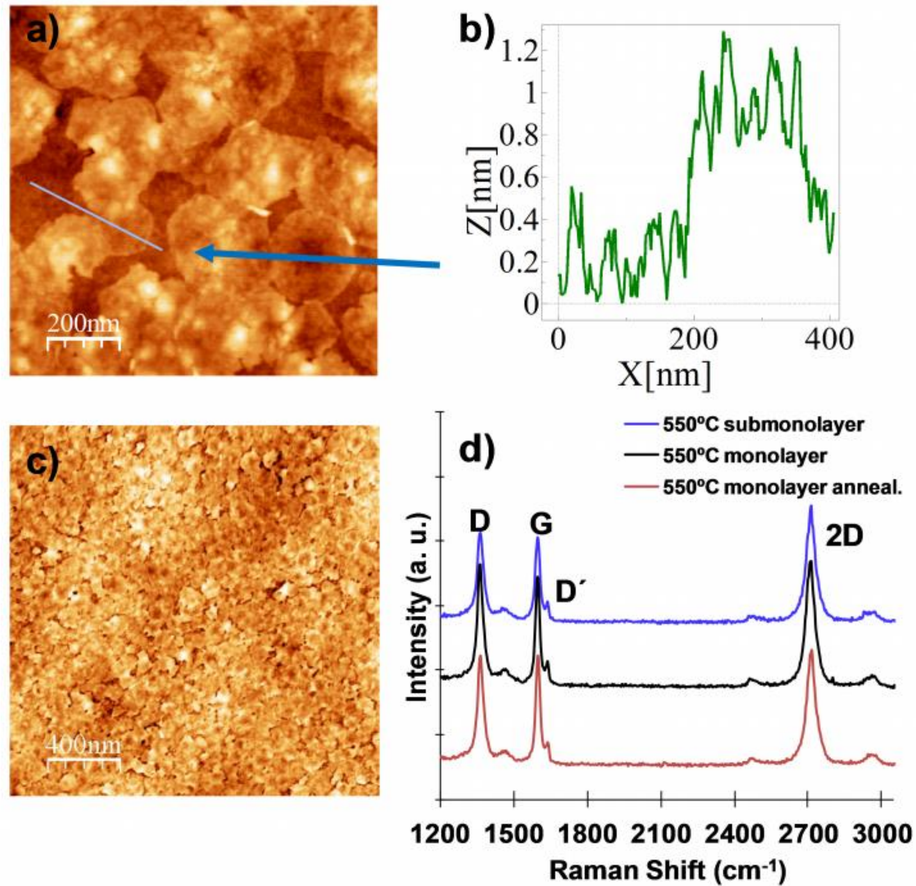

Fig. 4 a) AFM topographic image of graphene nuclei at 550 ºC, H_2/C_2H_2 = 50/0.9:0.8 (sccm), $P_T = 5.4\times10^{-2}$ mbar: P = 200 W, t_1 = 5 min t_2 = 7 h. Vertical scale: 0-5 nm b) Corresponding profile from a graphene flake in a). c) Continuous film, t_2 = 10h and same conditions than a). Vertical scale: 0-5 nm. d) Corresponding Raman spectrum of sample (a) (blue) and (c) before (black) and after annealing (red).

The decrease of the sheet resistance after annealing could be also related to the same reason, H species desorption from grains and boundaries and conversion of carbon hybridization.[47, 55, 57] In order to check this sp^3 to sp^2 conversion, we performed some XPS measurements in the annealed sample that were compared with the routine XPS

analysis done before annealing. Figure 5 presents the derivative of the C_{KVV} Auger peak before and after annealing the sample at 580 ºC in UHV. While the XPS C 1s core level peak presents basically the same shape before and after annealing (see supporting S4), the derivative of the C_{KVV} Auger peak presents a broadening. The distance between the maximum and the minimum of the derivative spectra in figure 5, also known as D value (eV.),[58] increases after annealing from 18.8 eV to values close to 23 eV. This increase upon annealing points towards a sp^2 conversion that leads to a final graphene film exhibiting mostly sp^2 hybridization.

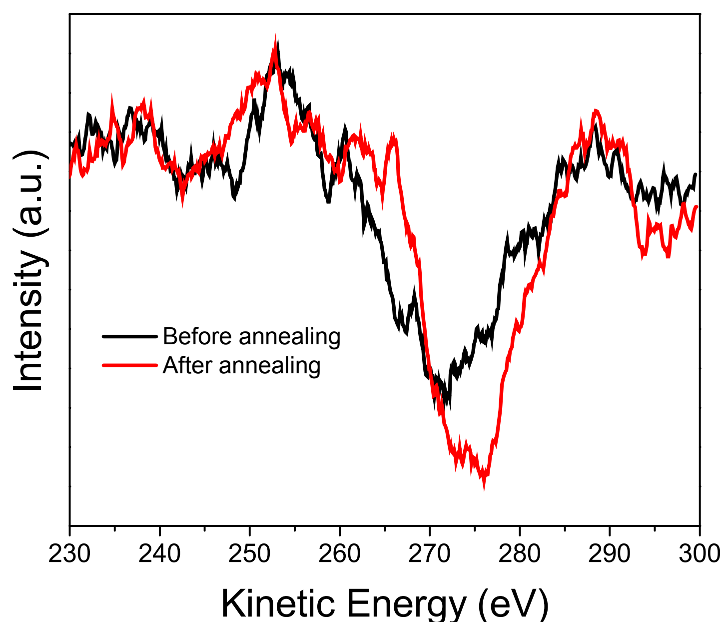

Fig. 5 Auger CKVV peak derivative from the sample grown at 550 ºC, before (black) and after annealing (red) at 580 ºC in UHV.

An alternative growth protocol was carried out at higher temperature, 650 ºC, during the first and second steps of the synthesis. As the nucleation rate at this temperature is much higher than at 550 ºC, t_2 is prolonged only for 150 min. It is important to note that this

was the minimum time to deposit a continuous film with these thermodynamic parameters. Figure 6(a) presents the morphology of the film grown under these conditions. It can be observed that, as the nucleation density is extremely high, the average domain lateral size is less than 30 nm. However, the grain size has increased slightly in comparison with that of figure 1(a), where the deposit was performed with similar conditions for 90 min. Figure 6(b) depicts a lower magnification image of the same sample where, at the center of the image, the AFM tip was used to sweep away the deposited material in order to measure the thickness of the film. This is achieved by switching to contact mode and increasing the applied force to remove the graphene layer. Figure 6(d) shows the line profile where it can be observed that the typical height of the film is around 2 nm, which doubles the thickness of the samples grown at 550 ºC. The continuity of this film was checked by four point probe measurements. The average sheet resistance was around 3.3 k ·sq^{-1}. This value decreased further down to 1.8 k ·sq^{-1} after annealing the sample at 650 ºC in vacuum at 10^{-6} mbar which, even considering the double thickness of the layer, shows a clear improvement regarding the layer grown at 550 ºC. Figure 6(c) presents a comparison of the Raman spectra of the as grown film (in red) along with the spectrum of the same sample after annealing (black). Both spectra show the typical peaks of graphene films. The intensity ratio I_{2D}/I_G is around 0.3-0.4 in both spectra and the 2D peak is not completely symmetric with FWHM of 55 cm^{-1}. This corresponds to a few layer graphene. The most remarkable difference between the Raman spectra appears in the intensity ratio I_D/I_G after annealing. In the as grown sample I_D/I_G 1, a high expected value due to the extremely high density of grain boundaries, as we previously commented on figure 4(d). After annealing, I_D/I_G decreases approximately to 0.7. This is again the signature of H desorption from the film and conversion to sp^2. This would confirm that, in addition to the large density of grain boundaries, H functionalization of the graphene boundaries inducing a sp^3 configuration is an important contribution for the increase in the intensities of the D and D´ peaks. The same phenomenology is observed in the growth of graphene on quartz and glass and explained through the reaction path as followed by DFT calculations. [47]

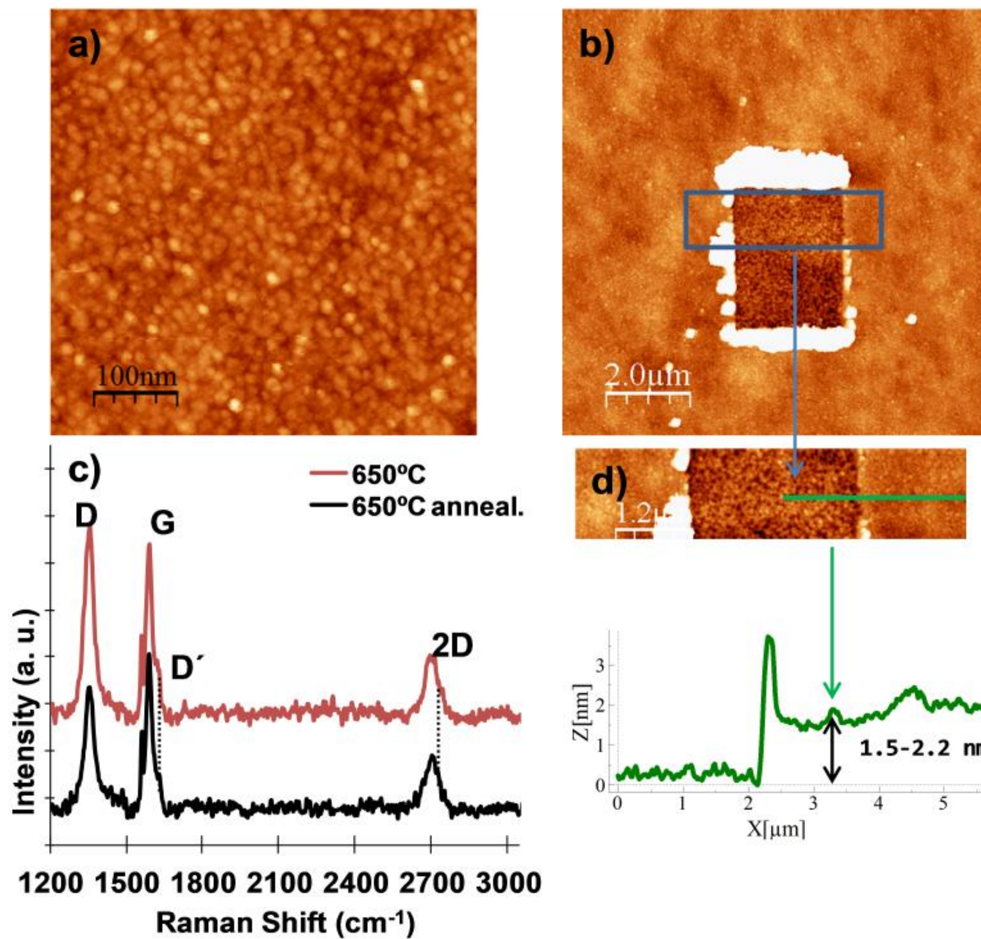

Figure 6 a) AFM topographic image of graphene continuous film at 650 ºC, H_2/C_2H_2 = 50/0.5:0.4 (sccm), P_T = 5.4×10^{-2} mbar: P = 200 W, t_1 = 5 min t_2 = 150 min. Vertical scale: 0-3 nm. b) Large scan image of sample in a) showing at the center the swept area where graphene film has been removed with the AFM tip. Vertical scale: 0-10 nm. c) Corresponding Raman spectrum of sample c), before (red line) and after annealing in vacuum (black line). d) Height profile (below) corresponding to the marked line in the topographic image (above).

Differences in the resistance measured for the sample grown at T=550ºC and T= 650ºC can be related to:

i) Bad stitching between grains. In fig 4(c), it is already apparent that there exist dark regions corresponding to tiny uncovered areas in the sample grown at T=550ºC (see

supplementary, Fig. S6). These bare areas do not appear in the sample grown at 650ºC where a thicker layer enables always a graphene path for carriers.

ii) Quality of the intrinsic properties of the grains. It has been reported[56, 59] that at temperatures around 500ºC the functionalization of graphene by the hydrogen species of the plasma is most efficient, decreasing the reactivity as the temperature is increased. Therefore, the intrinsic quality of the graphene grown at lower temperature may be worse than that of graphene grown at higher temperature.

Table 1 below, presents the final values of sheet resistance and resistivity after annealing (taking into account the measured thickness of the film) of this work. Previously published data are also included for comparison. Figure 7 shows jointly the dependence of the grain size and the nucleation density with the temperature. It is remarkable to observe how grain size decreases over one order of magnitude and nucleation density expands over three orders of magnitude. Comparing the properties of the graphene films fabricated at 550 ºC and 650 ºC on the Si/SiO_x, there are some crucial aspects to take into account. The resistivity is higher at 550ºC even with grains one order of magnitude larger than at high temperature, as the low temperature does not promote any diffusive process at the substrate surface. At the lower temperature, although monolayer graphene islands with well-defined shapes are formed and the coalescence is apparent in many grain boundaries, in some other points the random orientation of the grains grown impedes the perfect matching between them so as to form a continuous film with complete stitching that influences the film properties. Higher temperature favors graphitization, increases thickness and, apparently, the coalescence of tiny grains. Even though the grain size is quite small, there is an improvement in terms of resistance and resistivity in the films deposited at 650 ºC. Table 1 confirms that in both cases, the resistivity of the films improves recently published results.

Table 1. Sheet resistance (**R**) and resistivity ( ) of graphene directly grown on Si/SiOx.

Ref.	**Deposition**		**R**	
	Technique	**T(ºC)**	**(·sq^{-1})**	**(·m)**
This work	ECR-CVD	650	1800	$3.6 \cdot 10^{-6}$
		550	8000	$6.4 \cdot 10^{-6}$
[35]	AP-CVD$^{(i)}$	1000	13300	$2.6 \cdot 10^{-5}$
[38]	AP-CVD	1200	16540	$5.6 \cdot 10^{-6(iii)}$
[42]	PE-CVD(ii)	585	32700	$4.9 \cdot 10^{-5}$
[60]	CVD$^{(iv)}$	950	see[60]	$2 \cdot 10^{-5}$

(i)Atmospheric pressure pyrolytic CVD (AP-CVD), 2 nm height.

(ii) Bilayer graphene, 1.5 nm height

(iii)Sample thickness calculated from optical transmittance data.

(iv)Low pressure CVD. A range of values is given for various film thicknesses (<5nm in all cases).

Finally, it is noteworthy that the annealing treatment at 650 ºC carried out on the films grown at both temperatures induces an improvement of the conductivity of the films due to an increase in the sp^2 carbon hybridization. In both cases, the sheet resistance is reduced nearly to the half of the original value with the annealing treatment.

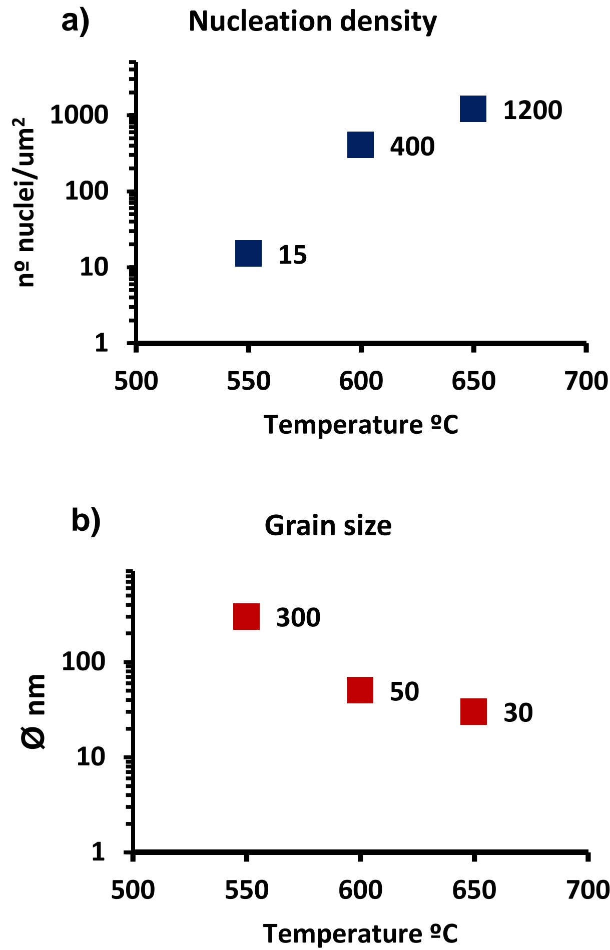

Figure 7. Summary of main results of nucleation density (a) and grain size (b) vs. temperature of this work. The results have been extracted from the previous figures and are approximate.

Conclusions

The direct growth of monolayer and few layer graphene films on thin silicon oxide/Si substrate at low temperature following two step synthesis has been demonstrated using ERC-CVD techniques. At the lower temperature growth explored (550 ºC), monolayer graphene films exhibit typically grain size over 300 nm with high crystallinity. The nucleation density at this temperature is easily controlled but the grains and domain boundaries are functionalized with H species that can be desorbed with an annealing treatment to a large extent. However, the continuous film at this temperature suffers from poor stitching in some points due to random orientation of the grains and lack of

diffusion of species on the substrate surface. Nonetheless, the electrical properties of the film are useful for a range of applications. Increasing the temperature to 650 ºC, the nucleation density is poorly controlled due to the high efficiency in these experimental conditions and the resulting average grain size is one order of magnitude smaller with thicker few layer grains. However, the final conductive properties of the films with markedly low sheet resistance value (1800 $\cdot$sq^{-1}) are improved, probably due to the favored graphitization, coalescence and thickness. In this case, an annealing treatment also favors H desorption. No noticeable damage of the substrate was detected. Furthermore, the protocol developed at low temperature is scalable and avoids the transfer of the films. The results presented here represent a step forward in graphene integration for a variety of applications.

Conflicts of interest

There are no conflicts of interest to declare.

Acknowledgements

R. M. specially acknowledges scientific, technical and administrative support from Universidad Nacional de Educación a Distancia (**UNED**) in the framework of the PhD. Program in Sciences. ERC-synergy program funding (grant ERC-2013-SYG-610256 Nanocosmos), Spanish MINECO MAT2014-59772-C2-2-P funding and EU Graphene Flagship funding (Grant Graphene Core2 785219) are acknowledged. C. M. acknowledges the financial support by the 'Ramón y Cajal' Program of MINECO (RYC-2014-16626). Authors acknowledge Dr. A. del Campo for technical support with Raman measurements.

References

1. K. S. Novoselov, A. K. Geim, S. V. Morozov, D. Jiang, Y. Zhang, S. V. Dubonos, I. V. Grigorieva and A. A. Firsov, *Science*, 2004, **306**, 666-669.
2. K. S. Novoselov, A. K. Geim, S. V. Morozov, D. Jiang, M. I. Katsnelson, I. V. Grigorieva, S. V. Dubonos and A. A. Firsov, *Nature*, 2005, **438**, 197-200.

3. K. S. Novoselov, D. Jiang, F. Schedin, T. J. Booth, V. V. Khotkevich, S. V. Morozov and A. K. Geim, *Proceedings of the National Academy of Sciences of the United States of America*, 2005, **102**, 10451-10453.
4. R. R. Nair, P. Blake, A. N. Grigorenko, K. S. Novoselov, T. J. Booth, T. Stauber, N. M. R. Peres and A. K. Geim, *Science*, 2008, **320**, 1308-1308.
5. A. A. Balandin, S. Ghosh, W. Bao, I. Calizo, D. Teweldebrhan, F. Miao and C. N. Lau, *Nano Letters*, 2008, **8**, 902-907.
6. C. Lee, X. Wei, J. W. Kysar and J. Hone, *Science*, 2008, **321**, 385-388.
7. S. Bae, H. Kim, Y. Lee, X. Xu, J.-S. Park, Y. Zheng, J. Balakrishnan, T. Lei, H. Ri Kim, Y. I. Song, Y.-J. Kim, K. S. Kim, B. Özyilmaz, J.-H. Ahn, B. H. Hong and S. Iijima, *Nature Nanotechnology*, 2010, **5**, 574.
8. A. C. Ferrari, F. Bonaccorso, V. Fal'ko, K. S. Novoselov, S. Roche, P. Boggild, S. Borini, F. H. L. Koppens, V. Palermo, N. Pugno, J. A. Garrido, R. Sordan, A. Bianco, L. Ballerini, M. Prato, E. Lidorikis, J. Kivioja, C. Marinelli, T. Ryhanen, A. Morpurgo, J. N. Coleman, V. Nicolosi, L. Colombo, A. Fert, M. Garcia-Hernandez, A. Bachtold, G. F. Schneider, F. Guinea, C. Dekker, M. Barbone, Z. Sun, C. Galiotis, A. N. Grigorenko, G. Konstantatos, A. Kis, M. Katsnelson, L. Vandersypen, A. Loiseau, V. Morandi, D. Neumaier, E. Treossi, V. Pellegrini, M. Polini, A. Tredicucci, G. M. Williams, B. Hee Hong, J.-H. Ahn, J. Min Kim, H. Zirath, B. J. van Wees, H. van der Zant, L. Occhipinti, A. Di Matteo, I. A. Kinloch, T. Seyller, E. Quesnel, X. Feng, K. Teo, N. Rupesinghe, P. Hakonen, S. R. T. Neil, Q. Tannock, T. Lofwander and J. Kinaret, *Nanoscale*, 2015, **7**, 4598-4810.
9. C. Berger, Z. Song, T. Li, X. Li, A. Y. Ogbazghi, R. Feng, Z. Dai, A. N. Marchenkov, E. H. Conrad, P. N. First and W. A. de Heer, *The Journal of Physical Chemistry B*, 2004, **108**, 19912-19916.
10. X. Li, W. Cai, J. An, S. Kim, J. Nah, D. Yang, R. Piner, A. Velamakanni, I. Jung, E. Tutuc, S. K. Banerjee, L. Colombo and R. S. Ruoff, *Science*, 2009, **324**, 1312-1314.
11. C. Wirtz, K. Lee, T. Hallam and G. S. Duesberg, *Chemical Physics Letters*, 2014, **595-596**, 192-196.
12. S. Kumar, N. McEvoy, T. Lutz, G. P Keeley, V. Nicolosi, C. Murray, W. Blau and G. Duesberg, *Gas phase controlled deposition of high quality large-area graphene films*, 2010.
13. Y. Chen, X. L. Gong and J. G. Gai, *Advanced Science*, 2016, **3**, 1500343.
14. G. Lupina, J. Kitzmann, I. Costina, M. Lukosius, C. Wenger, A. Wolff, S. Vaziri, M. Östling, I. Pasternak, A. Krajewska, W. Strupinski, S. Kataria, A. Gahoi, M. C. Lemme, G. Ruhl, G. Zoth, O. Luxenhofer and W. Mehr, *ACS Nano*, 2015, **9**, 4776-4785.
15. N. Lindvall, M. T. Cole and A. Yurgens, *Applied Physics Letters*, 2011, **98**, 252107.
16. J. Chen, Y. Guo, Y. Wen, L. Huang, Y. Xue, D. Geng, B. Wu, B. Luo, G. Yu and Y. Liu, *Advanced Materials*, 2013, **25**, 992-997.
17. J. Hwang, M. Kim, D. Campbell, H. A. Alsalman, J. Y. Kwak, S. Shivaraman, A. R. Woll, A. K. Singh, R. G. Hennig, S. Gorantla, M. H. Rümmeli and M. G. Spencer, *ACS Nano*, 2013, **7**, 385-395.

18. H. J. Song, M. Son, C. Park, H. Lim, M. P. Levendorf, A. W. Tsen, J. Park and H. C. Choi, *Nanoscale*, 2012, **4**, 3050-3054.
19. K. Saito and T. Ogino, *The Journal of Physical Chemistry C*, 2014, **118**, 5523-5529.
20. S. K. Jerng, D. S. Yu, Y. S. Kim, J. Ryou, S. Hong, C. Kim, S. Yoon, D. K. Efetov, P. Kim and S. H. Chun, *The Journal of Physical Chemistry C*, 2011, **115**, 4491-4494.
21. X. Ding, G. Ding, X. Xie, F. Huang and M. Jiang, *Carbon*, 2011, **49**, 2522-2525.
22. S. Tang, H. Wang, H. S. Wang, Q. Sun, X. Zhang, C. Cong, H. Xie, X. Liu, X. Zhou, F. Huang, X. Chen, T. Yu, F. Ding, X. Xie and M. Jiang, 2015, **6**, 6499.
23. N. Mishra, V. Miseikis, D. Convertino, M. Gemmi, V. Piazza and C. Coletti, *Carbon*, 2016, **96**, 497-502.
24. W. Strupinski, K. Grodecki, A. Wysmolek, R. Stepniewski, T. Szkopek, P. E. Gaskell, A. Grüneis, D. Haberer, R. Bozek, J. Krupka and J. M. Baranowski, *Nano Letters*, 2011, **11**, 1786-1791.
25. J. Sun, T. Gao, X. Song, Y. Zhao, Y. Lin, H. Wang, D. Ma, Y. Chen, W. Xiang, J. Wang, Y. Zhang and Z. Liu, *Journal of the American Chemical Society*, 2014, **136**, 6574-6577.
26. J.-H. Lee, E. K. Lee, W.-J. Joo, Y. Jang, B.-S. Kim, J. Y. Lim, S.-H. Choi, S. J. Ahn, J. R. Ahn, M.-H. Park, C.-W. Yang, B. L. Choi, S.-W. Hwang and D. Whang, *Science*, 2014, **344**, 286-289.
27. J. Dai, D. Wang, M. Zhang, T. Niu, A. Li, M. Ye, S. Qiao, G. Ding, X. Xie, Y. Wang, P. K. Chu, Q. Yuan, Z. Di, X. Wang, F. Ding and B. I. Yakobson, *Nano Letters*, 2016, **16**, 3160-3165.
28. J. Sun, Y. Chen, M. K. Priydarshi, Z. Chen, A. Bachmatiuk, Z. Zou, Z. Chen, X. Song, Y. Gao, M. H. Rümmeli, Y. Zhang and Z. Liu, *Nano Letters*, 2015, **15**, 5846-5854.
29. Z. Chen, B. Guan, X.-d. Chen, Q. Zeng, L. Lin, R. Wang, M. K. Priydarshi, J. Sun, Z. Zhang, T. Wei, J. Li, Y. Zhang, Y. Zhang and Z. Liu, *Nano Research*, 2016, **9**, 3048-3055.
30. B. Wang, B. V. Cunning, S.-Y. Park, M. Huang, J.-Y. Kim and R. S. Ruoff, *ACS Nano*, 2016, **10**, 9794-9800.
31. J. Sun, Y. Chen, M. K. Priydarshi, T. Gao, X. Song, Y. Zhang and Z. Liu, *Advanced Materials*, 2016, **28**, 10333-10339.
32. Y. Chen, J. Sun, J. Gao, F. Du, Q. Han, Y. Nie, Z. Chen, A. Bachmatiuk, M. K. Priydarshi, D. Ma, X. Song, X. Wu, C. Xiong, M. H. Rümmeli, F. Ding, Y. Zhang and Z. Liu, *Advanced Materials*, 2015, **27**, 7839-7846.
33. C. Martin-Olmos, H. I. Rasool, B. H. Weiller and J. K. Gimzewski, *ACS Nano*, 2013, **7**, 4164-4170.
34. J. Pang, R. G. Mendes, P. S. Wrobel, M. D. Wlodarski, H. Q. Ta, L. Zhao, L. Giebeler, B. Trzebicka, T. Gemming, L. Fu, Z. Liu, J. Eckert, A. Bachmatiuk and M. H. Rümmeli, *ACS Nano*, 2017, **11**, 1946-1956.
35. N. Lindvall, M. T. Cole, T. J. Booth, P. Bøggild, J. Liu and A. Yurgens, *Journal of Applied Physics*, 2012, **111**, 044103.

36. J. Chen, Y. Guo, L. Jiang, Z. Xu, L. Huang, Y. Xue, D. Geng, B. Wu, W. Hu, G. Yu and Y. Liu, *Advanced Materials*, 2014, **26**, 1348-1353.
37. S. C. Xu, B. Y. Man, S. Z. Jiang, C. S. Chen, C. Yang, M. Liu, X. G. Gao, Z. C. Sun and C. Zhang, *CrystEngComm*, 2013, **15**, 1840-1844.
38. H. Bi, S. Sun, F. Huang, X. Xie and M. Jiang, *Journal of Materials Chemistry*, 2012, **22**, 411-416.
39. J. Chen, Y. Wen, Y. Guo, B. Wu, L. Huang, Y. Xue, D. Geng, D. Wang, G. Yu and Y. Liu, *Journal of the American Chemical Society*, 2011, **133**, 17548-17551.
40. N.-E. Weber, A. Binder, M. Kettner, S. Hirth, R. T. Weitz and Ž. Tomovi , *Carbon*, 2017, **112**, 201-207.
41. H. Iwai, *Microelectron. Eng.*, 2009, **86**, 1520-1528.
42. D. Liu, W. Yang, L. Zhang, J. Zhang, J. Meng, R. Yang, G. Zhang and D. Shi, *Carbon*, 2014, **72**, 387-392.
43. Y. S. Kim, K. Joo, S.-K. Jerng, J. H. Lee, E. Yoon and S.-H. Chun, *Nanoscale*, 2014, **6**, 10100-10105.
44. J. Sun, M. E. Schmidt, M. Muruganathan, H. M. H. Chong and H. Mizuta, *Nanoscale*, 2016, **8**, 6659-6665.
45. S. Chugh, R. Mehta, N. Lu, F. D. Dios, M. J. Kim and Z. Chen, *Carbon*, 2015, **93**, 393-399.
46. S. F. Yoon, K. H. Tan, J. Rusli, Ahn and Q. F. Huang, *Diamond and Related Materials*, 2000, **9**, 2024-2030.
47. R. Muñoz, C. Munuera, J. I. Martínez, J. Azpeitia, C. Gómez-Aleixandre and M. García-Hernández, *2D Materials*, 2017, **4**, 015009.
48. M. Roberto and G.-A. Cristina, *Journal of Physics D: Applied Physics*, 2014, **47**, 045305.
49. M. A. Lieberman and A. J. Lichtenberg, *Principles of Plasma Discharges and Materials Processing*, 2005.
50. I. Horcas, R. Fernández, J. M. Gómez-Rodríguez, J. Colchero, J. Gómez-Herrero and A. M. Baro, *Review of Scientific Instruments*, 2007, **78**, 013705.
51. M. Nishijima, J. Yoshinobu, H. Tsuda and M. Onchi, *Surface Science*, 1987, **192**, 383-397.
52. S. Riikonen, A. V. Krasheninnikov, L. Halonen and R. M. Nieminen, *The Journal of Physical Chemistry C*, 2012, **116**, 5802-5809.
53. P. Wu, W. Zhang, Z. Li, J. Yang and J. G. Hou, *The Journal of Chemical Physics*, 2010, **133**, 071101.
54. *Proceedings of the Royal Society of London. Series A. Mathematical and Physical Sciences*, 1964, **280**, 139-152.
55. D. C. Elias, R. R. Nair, T. M. G. Mohiuddin, S. V. Morozov, P. Blake, M. P. Halsall, A. C. Ferrari, D. W. Boukhvalov, M. I. Katsnelson, A. K. Geim and K. S. Novoselov, *Science*, 2009, **323**, 610-613.
56. G. Diankov, M. Neumann and D. Goldhaber-Gordon, *ACS Nano*, 2013, **7**, 1324-1332.

57. Y. Wang, X. Xu, J. Lu, M. Lin, Q. Bao, B. Özyilmaz and K. P. Loh, *ACS Nano*, 2010, **4**, 6146-6152.

58. J. C. Lascovich and S. Scaglione, *Applied Surface Science*, 1994, **78**, 17-23.

59. Y. Rong, Z. Lianchang, W. Yi, S. Zhiwen, S. Dongxia, G. Hongjun, W. Enge and Z. Guangyu, *Advanced Materials*, 2010, **22**, 4014-4019.

60. N. McEvoy, N. Peltekis, S. Kumar, E. Rezvani, H. Nolan, G. P. Keeley, W. J. Blau and G. S. Duesberg, *Carbon*, 2012, **50**, 1216-1226.